Atom Indonesia

The Quantitative Effect of Noise and Object Diameter on Low-Contrast Detectability of AAPM CT Performance Phantom Images

E. Setiawati[1], C. Anam[1,*], W. Widyasari[1], G. Dougherty[2]

[1]*Department of Physics, Faculty of Sciences and Mathematics, Diponegoro University, Semarang 50275, Indonesia*
[2]*Department of Applied Physics and Medical Imaging, California State University Channel Islands, Camarillo, CA 93012, USA*

ARTICLE INFO

ABSTRACT

Parameters for determining computed tomography (CT) image quality include noise and low-contrast detectability. Studies on low-contrast detectability using the AAPM CT performance phantom have several limitations, such as the absence of quantitative information on the effect of noise and object size on low-contrast detectability. In this study, the quantitative effect of noise and object diameter on low-contrast detectability were investigated. Images of the American Association of Physicists in Medicine (AAPM) CT performance phantom model 610 were acquired with a tube voltage of 120 kV and tube currents of 50, 100, 150, and 200 mA. The low-contrast section of the AAPM CT performance phantom model 610 has objects with diameters between 2.5 and 7.5 mm. We analysed the mean CT number, noise level, signal-to noise ratio (SNR), and contrast-to-noise ratio (CNR), acquired using MatLab software. The results obtained indicate that noise and object size affect low-contrast detectability. The CNRs increase linearly with increasing of object diameter with R^2 of 0.88, 0.67, 0.75, and 0.83 for tube currents of 50, 100, 150 and 200 mA, respectively.

INTRODUCTION

Computed tomography (CT) is a diagnostic tool using X-rays with computerized techniques to obtain internal tomographic images of the human body. CT is widely used for early and accurate diagnosis of many abnormalities. It is worth noting that CT image-based accurate diagnosis results have to be supported by good image quality [1]. The key parameters for determining image quality include noise level and low-contrast detectability [2]. Noise is a fluctuation in pixel values that appear randomly in the image [3], while low-contrast detectability is the ability of the imaging system to differentiate the smallest contrast difference among tissues (objects) having very small size [4,5]. One advantage of CT image over other modalities is its low-contrast detectability [6,7]. Image of CT can distinguish between objects having a contrast of only about 0.5 % [8,9].

The noise level in an image can be expressed as the signal-to-noise ratio (SNR) [10]. SNR is the ratio of the magnitude of the signal amplitude to the noise. SNR increases when the signal amplitude increases or when image noise decreases [11]. The noise level and low-contrast detectability can be expressed simultaneously in a contrast-to-noise ratio (CNR) [12]. Increases in SNR and CNR values indicate lower noise level and improved image quality [10]. SNR and CNR are usually measured on relatively wide objects [13]. Studies on SNR and CNR on CT images have been carried out using several phantoms, including the ACR CT phantoms [14], pediatric phantom [7], AAPM CT performance phantom model 76-410 [15,16], and AAPM CT performance phantom model 610 [17].

The AAPM CT performance phantom model 76-410 and model 610 have differences in the low-contrast section. The AAPM CT performance phantom model 76-410 has six different object diameters, i.e., 25.4, 19.1, 12.7, 9.5, 6.4, and 3.2 mm, while the AAPM CT performance phantom model 610 has diameters from 7.5 to 2.5 mm, with a diameter difference between objects of 0.5 mm, i.e.,

eleven objects with different diameters [18]. Both models are made of solid acrylic with a mean value of +10 HU, and the holes are filled with water with a mean value of 0 HU [15,18].

Park et al. [15] and Noh et al. [16] studied low-contrast detectability at a tube voltage of 120 kV and a tube current of 250 mA, while Rozanah et al. [17] used tube currents of 180 mA and 350 mA. In these and similar studies, the effect of noise and object size on low-contrast detectability were not investigated. In other studies [19,20], it is reported that object diameter has an obvious impact on low-contrast detectability. However, the phenomenon is usually observed by visual observation. The visual observation of low-contrast on various small object size is subjective and leads to intra- and inter-variabilities. To reduce these variabilities, many studies employing statistical methods have been carried out to investigate the low-contrast detectability [21-24]. Statistical low-contrast detectability can be measured on homogeneous image phantom by applying a dedicated computer software package [25]. However, many CT centers do not have the software package for measuring the statistical low-contrast detectability. Hence, investigation of quantitative low-contrast detectability on low-contrast section of readily-available commercial physical phantom is important. To the best of our knowledge, there is no study on the quantitative impact of object size on low-contrast section of AAPM CT performance image. Drawing many regions of interest (ROIs) on many small low-contrast object within the image of the AAPM CT performance phantom is laborious and time consuming. The aim of current study is to quantitatively evaluate the effect of noise and object size on low-contrast detectability on the AAPM CT performance phantom model 610.

MATERIALS AND METHODS

Images of AAPM CT performance phantom

An example image of the low-contrast section of the AAPM Model 610 CT performance phantom (CIRS, Norfolk, USA) is shown in Fig. 1. The basic material of the phantom is solid acrylic having a mean value of ~10 HU [15,18]. This phantom consists of air-filled holes with diameters of 2.5 mm to 7.5 mm. The difference in diameter between objects is 0.5 mm, so that in total there are eleven different object diameter sizes. Each diameter size consists of 4 to 5 objects [18]. In general, low-contrast measurement usually uses water, with a mean value of ~0 HU [15]. In addition to water,

other fillings can be a solution of sodium chloride and water or dextrose and water. On the phantom, there is a wide triangular object, which can be used to measure SNR and CNR which is not affected by size.
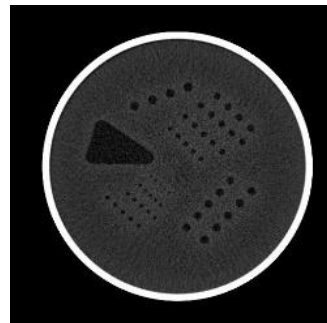

Fig. 1. Example image of low-contrast part of AAPM CT performance phantom model 610.

The phantom was scanned with a Revolution Evo CT scanner (GE Healthcare, Waukesha, USA). Scanning parameters are listed in Table 1. To obtain different noise levels, the tube current was varied from 50 mA to 200 mA with a fixed tube voltage of 120 kV.

Table 1. Scan parameters.

Parameters	Value
Acquisition mode	Axial
Tube voltage (kV)	120
Tube current (mA)	50, 100, 150, and 200
Slice thickness (mm)	5
Window width (HU)	100
Window levels (HU)	40
Pitch	0.984
Rotation time (s)	2
Field of view (FoV) (cm)	25.5
Reconstruction method	FBP

Measuring mean CT number and noise

The mean CT number and noise values of objects (i.e., water) and background (i.e., acrylic) were measured using MATLAB R2018a (MathWorks Inc., Natick, USA). We wrote a graphical user interface (GUI) to easily measure mean CT number and noise as shown in Fig. 2. The process of measuring mean CT number and noise levels was manually carried out by placing ROIs on the image carefully adjusting them to be slightly smaller than the size of the objects. This ensures that the measured mean CT number and noise values are not affected by the background. An example of image with ROIs on each object is displayed in Fig. 3. Each measurement is repeated three times.
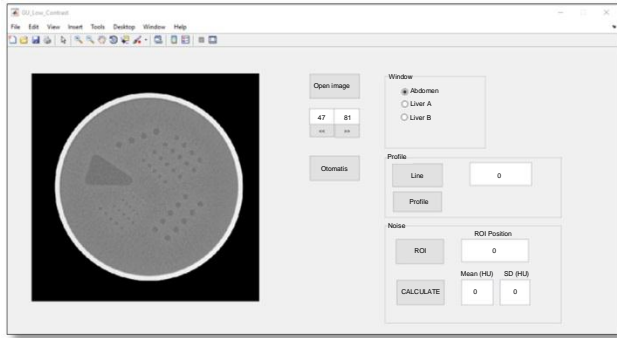
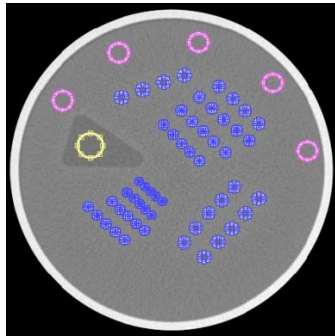**Fig. 2**. GUI displays mean and noise level measurements.

Fig. 3. Region of interests (ROIs) are located manually on AAPM CT performance phantom images, in order to measure CT number and noise of the objects (indicated by blue colour) and background (indicated by purple colour).

Calculation of SNR and CNR

Calculation of the SNR value was carried out after obtaining the results of the mean CT number and noise of the objects and background. Calculation of the SNR was carried out using Eq. (1) and calculation of the CNR value was carried out using Eq. (2).

$$SNR = \frac{\overline{CTN_o}}{\sigma_o} \tag{1}$$

$$CNR = \frac{\overline{CTN_o} - \overline{CTN_b}}{0.5\,(\sigma_o + \sigma_b)} \tag{2}$$

In Eqs. (1) and (2), $\overline{CTN_o}$ is the CT number of the object, $\overline{CTN_b}$ is the CT number of the background, σ_o is the noise of the object, and σ_b is the noise of the background.

RESULTS AND DISCUSSION

Mean CT number

Graphs of the mean CT number (in HU) and object diameter for various tube currents (in mA) are shown in Fig. 4. The CT numbers of small objects containing water are within ± 6 HU. Previous study reported that CT number of water must be within

± 7 HU [15]. Figure 4 shows that the mean CT number decreases with increasing the object diameter. This phenomenon is observed at every tube current. The mean CT number measured is (-2.6 ± 1.3) HU at 50 mA, (-1.3 ± 1.0) HU at 100 mA, (-1.8 ± 0.6) HU at 150 mA, and (-2.1 ± 0.7) HU at 200 mA. The mean CT number of background at each current was about 10 HU as expected [15,18]. The mean CT number increases with increasing the object diameter because the CT number of object is affected by the background. The CT number of the object is closer to the CT number of the background as the object becomes smaller.
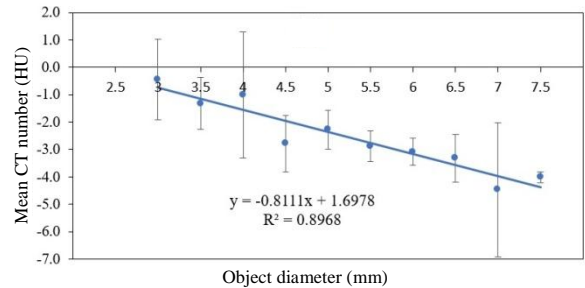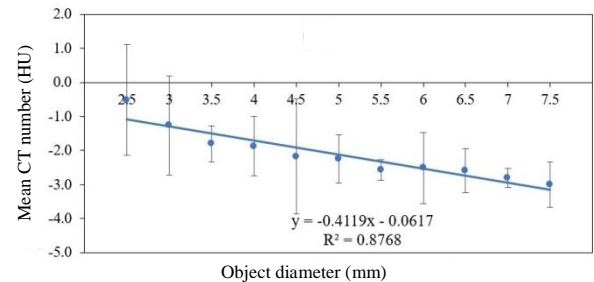

(a)
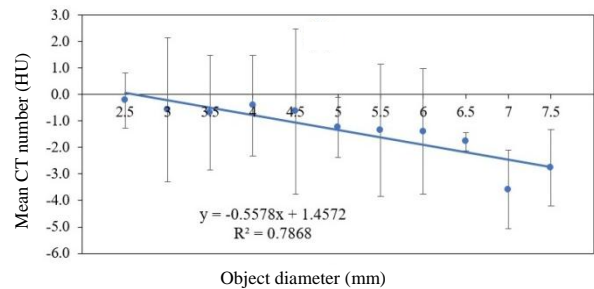
(b)
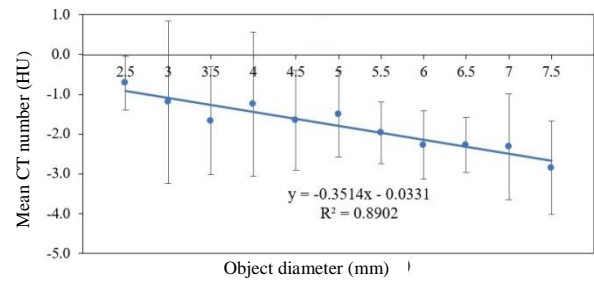
(c)

(d)

Fig. 4. The relationship between mean CT number and object diameter for various tube currents: (a) 50 mA, (b) 100 mA, (c) 150 mA, and (d) 200 mA.

Noise

Graphs of the noise (in HU) with object diameter for various tube currents (in mA) are shown in Fig. 5. The graph show a very weak correlation ($R^2 < 0.3$), indicating that the noise is independent of object diameter. The magnitude of the measured noise values for each tube current in both the object and the background is shown in Table 2. As expected the noise decreases with increasing tube current [26]. This is because the increasing tube current leads to increasing X-ray intensity, and it leads to decreasing quantum noise.
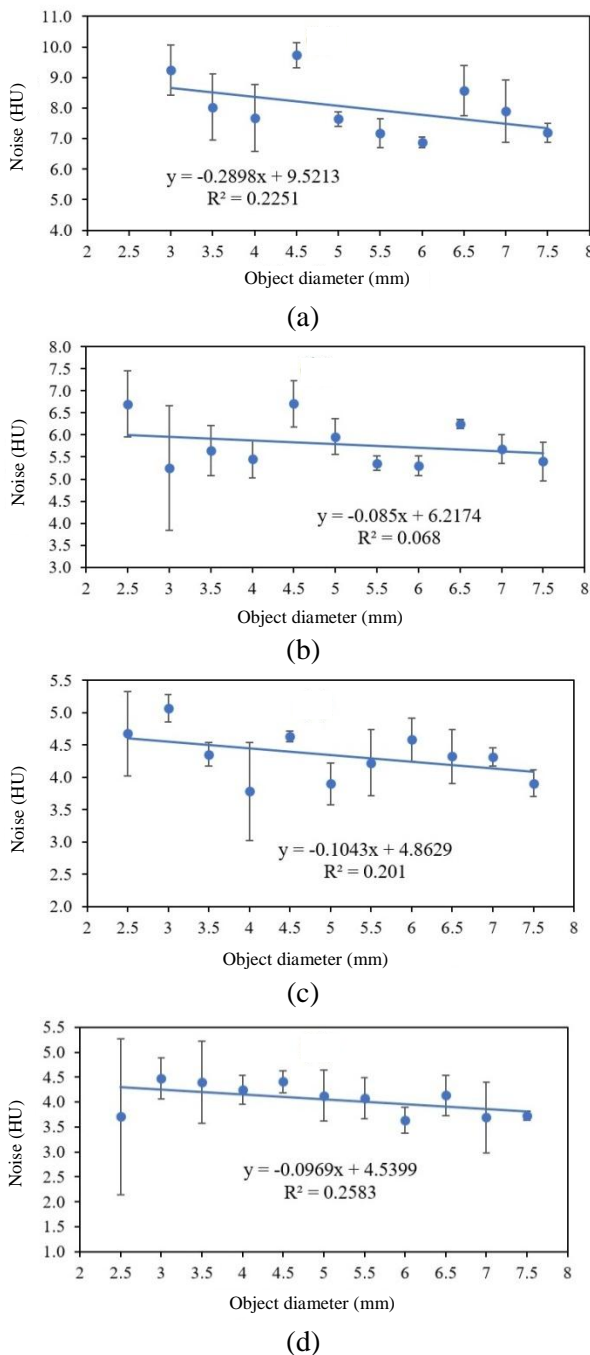
Table 2. Measured noise on a wide triangular object and background in every tube current

Tube current (mA)	Noise (HU)	
	Object	Background
50	8.2 ± 1.0	6.9 ± 0.7
100	5.5 ± 0.2	4.6 ± 0.3
150	4.4 ± 0.3	3.6 ± 0.1
200	3.6 ± 0.7	3.4 + 0.2

It is important to note that the noise in the background is smaller than that in the object. This is because noise in the background is influenced by the quantum noise, while noise in the object is also influenced by nonuniformity of material composition [27].

SNR

Graphs of the SNR and object diameter for various tube currents (in mA) are shown in Fig. 6. The graph show that SNR increases with increasing object diameter. The SNR also increases with an increase of tube current due to reduced noise. A higher SNR is an indication of better image quality. In this study, the highest SNR value is obtained from the highest tube current (i.e., 200 mA). It is well understood that the SNR value is proportional to the tube current [28]. Quantitatively, it was found that the image produced from 100 mA has much better quality than the 50 mA one. The smallest object of 2.5 mm cannot be observed at tube current of 50 mA due to the noise, while at a current of 100 mA the smallest object can still be observed.

CNR

The relationship between CNR and object diameter for various tube currents is shown in Fig. 7. It shows that CNR increases linearly with increasing of object diameter (R^2 values are 0.8764, 0.6742, 0.7456, and 0.8267 for tube currents of 50, 100, 150 and 200 mA, respectively). The CNR also increases with an increase of tube current. The CNR value is influenced by the tube current and the object diameter. A previous study conducted by Choi et al. [7] showed that the higher the tube current in the image, the greater the CNR value obtained.

In this study, the impact of the noise and the object diameter on low-contrast detectability of the AAPM CT performance phantom have been

Evaluated quantitatively. A GUI in MATLAB has been developed for measuring mean CT number, noise, SNR, and CNR. Measurements have been conducted on objects (i.e., water as filling material) and background (i.e., acrylic). Usually, evaluation

(a)

(b)

(c)

(d)

Fig. 5. The relationship between noise and object diameter for various tube currents: (a) 50 mA, (b) 100 mA, (c) 150 mA, and (d) 200 mA.

of low-contrast resolution is qualitatively conducted by visual evaluation [19, 20]. The visual evaluation is obviously subjective and leads to intra- and inter-variabilities.

However, in this study, the placement of ROIs on the objects was still determined manually. This approach, of course, is very tiring and time consuming, because there are as many as 54 small low-contrast objects and the ROIs have to be carefully located within them. In the next study, a method of placing ROIs automatically on low-contrast objects will be developed so that automatic low-contrast measurements will be easier, faster, and more efficient in clinical setting.
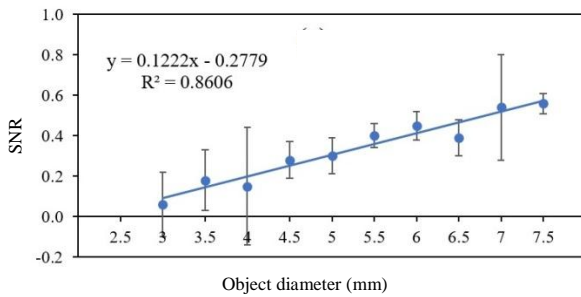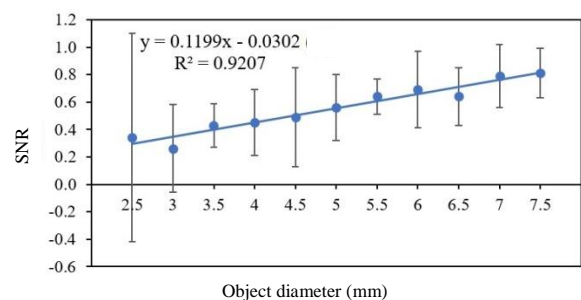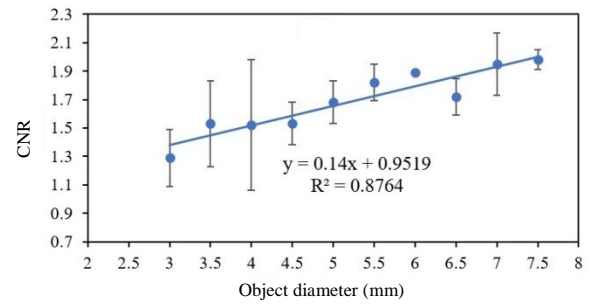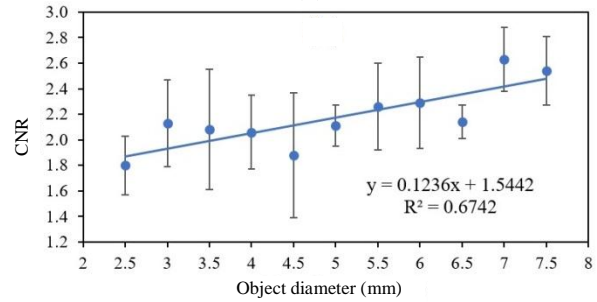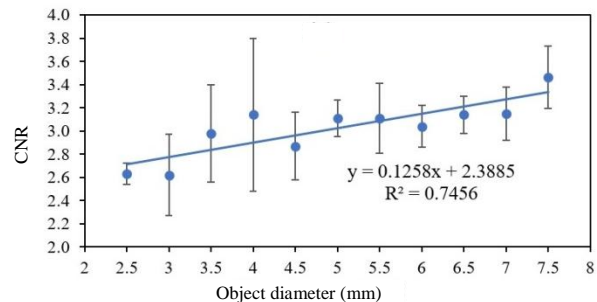
(a)
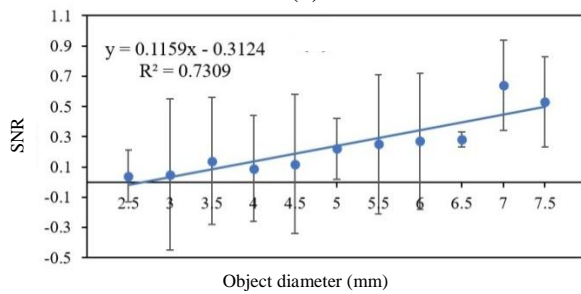
(b)
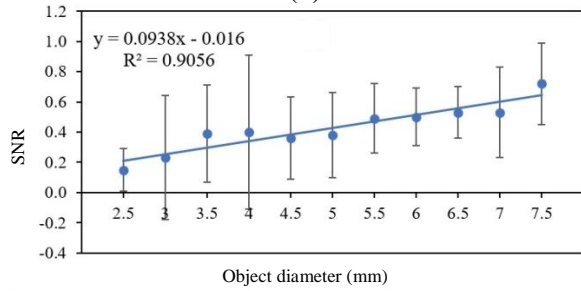
(c)

(d)

Fig. 6. The relationship between SNR and object diameter for various tube currents: (a) 50 mA, (b) 100 mA, (c) 150 mA, and (d) 200 mA.
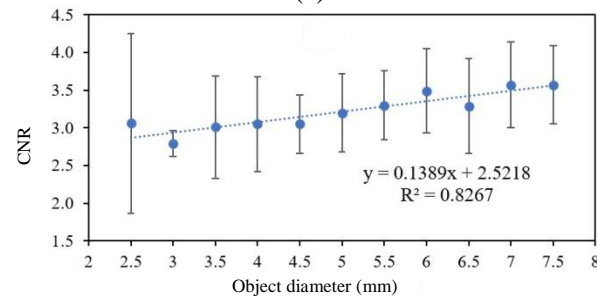
(a)

(b)

(c)

(d)

Fig. 7. Graphs of the relation between CNR and object diameter for various tube currents: (a) 50 mA, (b) 100 mA, (c) 150 mA, and (d) 200 mA.

CONCLUSION

The quantitative effects of noise and object diameter on low-contrast detectability have been investigated. The noise value and object diameter affect low-contrast detectability. Higher noise value leads to lower contrast detectability. The increase of object size diameter leads to an increase of the low-contrast detectability. The CNRs increase linearly with increasing of object diameter with R^2 of 0.8764, 0.6742, 0.7456, and 0.8267 for tube currents respectively 50, 100, 150, and 200 mA.

ACKNOWLEDGMENT

AUTHOR CONTRIBUTION

E. Setiawati and C. Anam conceived of the idea and contributed to study design. W. Widyasari and E. Setiawati collected the data and analysis. W. Widyasari and G. Dougherty wrote the manuscript. All authors read and approved the manuscript.

REFERENCES

1. P. Barca, F. Paolicchi, G. Aringhieri *et al.*, PLOS One **16** (2021) 1.

2. J. Conzelmann, U. Genske, A. Emig *et al.*, Eur. Radiol. **32** (2022) 1267.

3. C. Anam, H. Sutanto, K. Adi *et al.*, Biomed. Phys. Eng. Express. **6** (2020) 065001.

4. T. Njølstad, K. Jensen, A. Dybwad *et al.*, Eur. J. Radiol. Open. 9 (2022) 100418.

5. S. Riyanto, W. S. Budi and C. Anam, Berkala Fisika **22** (2019) 105. (in Indonesian)

6. S. T. Bache, P. J. Stauduhar, X. Liu *et al.*, J. Appl. Clin. Med. Phys. **18** (2017) 163.

7. H. R. Choi, R. E. Kim, C. W. Heo *et al.*, Optik 168 (2018) 54.

8. K. Gulliksrud, C. Stokke and A. C. T. Martinsen, Phys. Med. **30** (2014) 521.

9. C. Anam, W. S. Budi, F. Haryanto *et al.*, Sci. Vis. **11** (2019) 56.

10. Y. He, L. Zeng, W. Yu *et al.*, Med. Biol. Eng. Comput. **58** (2020) 2621.

11. F. van Ommen, F. Kauw, E. Bennink *et al.*, Acad. Radiol. **28** (2021) e323.

12. H. A. Alsleem and H. M. Almohiy, Med. Sci. **8** (2020) 26.

13. H. Li, S. Dolly, H. C. Chen *et al.*, J. Appl. Clin. Med. Phys. **17** (2016) 377.

14. Z. Mansour, A. Mokhtar, A. Sarhan *et al.*, Egypt. J. Radiol. Nucl. Med. **47** (2016) 1665.

15. H. J. Park, S. E. Jung, Y. J. Lee *et al.*, Korean J. Radiol. **10** (2009) 490.

16. S. S. Noh, H. S. Um and H. C. Kim, J. Inst. Electron. Inf. Eng. **51** (2014) 163.

17. R. Rozanah, W. Setiabudi and Z. Arifin, Youngster Physics Journal **4** (2015) 117. (in Indonesian)

18. CIRS, AAPM CT Performance Phantom Model 610: User Guide. CIRS Inc, USA (2012).

19. L. Bellesi, R. Wyttenbach, D. Gaudino *et al.*, Eur. Radiol. Exp. 1 (2017) 1.

20. L. Yu, B. Chen, J. M. Kofler *et al.*, Med. Phys. **44** (2017) 3990.

21. Y. Zhou, J. Appl. Clin. Med. Phys. **21** (2020) 128.

22. Y. Zhou, A. Scott II, J. Allahverdian *et al.*, Phys. Med. Biol. **60** (2015) 7671.

23. S. T. Bache, P. J. Stauduhar, X. Liu *et al.*, J. Appl. Clin. Med. Phys. **18** (2017) 163.

24. M. Chacko and S. Aldoohan, Med. Phys. **43** (2016) 3396.

25. C. Anam, A. Naufal, T. Fujibuchi *et al.*, J. Appl. Clin. Med. Phys. **23** (2022) e13719.

26. C. Anam, I. Arif, F. Haryanto *et al.*, J. Biomed. Phys. Eng. **11** (2021) 163.

27. I. Suyudi, C. Anam, H. Sutanto *et al.*, J. Biomed. Phys. Eng. **10** (2020) 215.

28. A. Mokhtar, Z. A. Aabdelbary, A. Sarhan *et al.*, J. Radiol. Nucl. Med. **52** (2021) 269.